Biomass Burning Smoke Influences Clouds over the Western U. S.

Cynthia H. Twohy[1]
Darin W. Toohey[2]
Ezra J. T. Levin[3,4]
Paul J. DeMott[3]
Bryan Rainwater[4]
Lauren A. Garofalo[5]
Matson A. Pothier[5]
Delphine K. Farmer[5]
Sonia M. Kreidenweis[3]
Rudra P. Pokhrel[6]
Shane M. Murphy[7]
J. Michael Reeves[8]
Kathryn A. Moore[3]
Emily V. Fischer[3]

1) NorthWest Research Associates, Bellevue, WA USA
2) Department of Atmospheric and Oceanic Sciences, University of Colorado, Boulder, CO USA
3) Department of Atmospheric Science, Colorado State University, Fort Collins, CO USA
4) Handix Scientific, Boulder, CO USA
5) Department of Chemistry, Colorado State University, Fort Collins, CO USA
6) Department of Physics, North Carolina A &T State University, Greensboro, NC, 27410
7) Department of Atmospheric Science, University of Wyoming, Laramie, WY USA
8) Research Aviation Facility, National Center for Atmospheric Research, Boulder, CO USA

Key Points

1) Western wildfires produce organic particles that readily act as cloud condensation nuclei due to their large size and partial hygroscopicity.
2) Wildfire smoke strongly impacts the microphysics of small cumulus clouds, which have high droplet concentrations and small droplet sizes.
3) Diverse impacts on radiative forcing and precipitation are possible over the western U.S. and downwind due to wildfire smoke.

Abstract

Small cumulus clouds over the western United States were measured via airborne instruments during the wildfire season in summer of 2018. Statistics of the sampled clouds are presented and compared to smoke aerosol properties. Cloud droplet concentrations were enhanced in regions impacted by biomass burning smoke, at times exceeding 3,000 cm^{-3}. Images and elemental composition of individual smoke particles and cloud droplet residuals are presented and show that most are dominantly organic, internally mixed with some inorganic elements. Despite their high organic content and relatively low hygroscopicity, on average about half of smoke aerosol particles >80 nm diameter formed cloud droplets. This reduced cloud droplet size in small, smoke-impacted clouds. A number of complex and competing climatic impacts may result from wide-spread reductions in cloud droplet size due to wildfires prevalent across the region during summer months.

Plain Language Summary

Wildfires over the western United States produce large quantities of smoke during the summer months. The smoke includes airborne particles that can act as nuclei for forming individual droplets in clouds. Particles and clouds in the region were sampled with a research aircraft to measure the properties of smoke particles and how they influenced the properties of small cumulus clouds. Clouds were strongly influenced by smoke across the western U.S. On average, sampled clouds had about 5x as many droplets, and droplets were about 1/2 the size, as in clouds not influenced by smoke. Because of their small droplet sizes, these smoky clouds are expected to reflect more light and produce less rain than clouds in clean air. Other complex effects are possible due to warming impacts of the smoke itself, and due to other potential impacts of smoke aerosols on larger, deeper clouds.

1 Introduction

Wildfires are abundant over the western United States during summer months, creating high concentrations of smoke aerosol particles that can impact health [*Künzli et al.*, 2006] and produce complex effects on climate over North America [*Jacobson*, 2014; *Brey et al.*, 2018]. The area burned by western U.S. wildfires has increased in recent years and is expected to increase further in a warmer future [*Westerling et al.*, 2006; *Dennison et al.*, 2014; *Abatzoglou and Williams*, 2016; *Westerling*, 2016; *Brey et al.*, 2020]. Smoke interactions with clouds in the region, however, are not well understood. Biomass burning smoke particles are dominated by organic material, usually internally mixed with some inorganic species [*Li et al.*, 2003; *Gomez et al.*, 2018]. Since inorganic compounds and some of the organic components in smoke particles are water-soluble [*Ruellan et al.*, 1999; *Gao et al.*, 2003; *Gomez et al.*, 2018], smoke particles usually have a low but non-negligible hygroscopicity parameter (kappa) [*Petters and Kreidenweis*, 2007]. Since biomass burning particles are usually in the accumulation mode with mean diameters >100 nm [*Reid et al.*, 2005], they have the potential to be cloud condensation nuclei (CCN) at modest supersaturations.

Particles from African savannah-derived smoke were shown to act as CCN by *Ross et al.* [2003], and smoke-derived CCN from the Amazon Basin were predicted to influence cloud properties with potentially significant cloud radiative forcing [*Roberts et al.*, 2003]. *Warner and Twomey* [1967] and *Eagan et al.* [1974] found that cumulus cloud droplet concentrations were enhanced by about a factor of 3 in smoke generated from Australian cane fires and Oregon forest fires, respectively. The latter study also noted smaller droplets and a narrower size distribution for smoke-influenced clouds. Over Amazonia, forest fire smoke was observed to reduce droplet size and precipitation at lower cloud levels, but can actually produce more ice-phase precipitation at higher levels in deep convection [*Andreae et al.*, 2004].

2 Experiment

Measurements of wildfire smoke plumes, aged smoke, and clouds influenced by smoke were sampled during the Western Wildfire Experiment for Cloud Chemistry, Aerosol Absorption, and Nitrogen (WE-CAN) during the summer of 2018. This was an active fire season in the region

(https://www.nifc.gov/fireInfo/nfn.htm), with California in particular being impacted by historically large and destructive fires (https://www.fire.ca.gov/stats-events/). The National Science Foundation /National Center for Atmospheric Research (NSF/NCAR) Hercules C-130 research aircraft (https://doi.org/10.5065/D6WM1BG0) was based in Boise, Idaho, and biomass burning smoke over much of the western U.S. was sampled (Fig. 1). Measurements of small altocumulus clouds with bases embedded in predominately aged smoke layers were made during six flights. Indirect aerosol effects on these small, midlevel cumulus clouds have not been extensively studied. Ambient pressures and temperatures at the level of cumulus penetration ranged from 485-660 mb and 260K to 275K, respectively. Additionally, one flight sampled warm stratocumulus clouds just off the California coast.

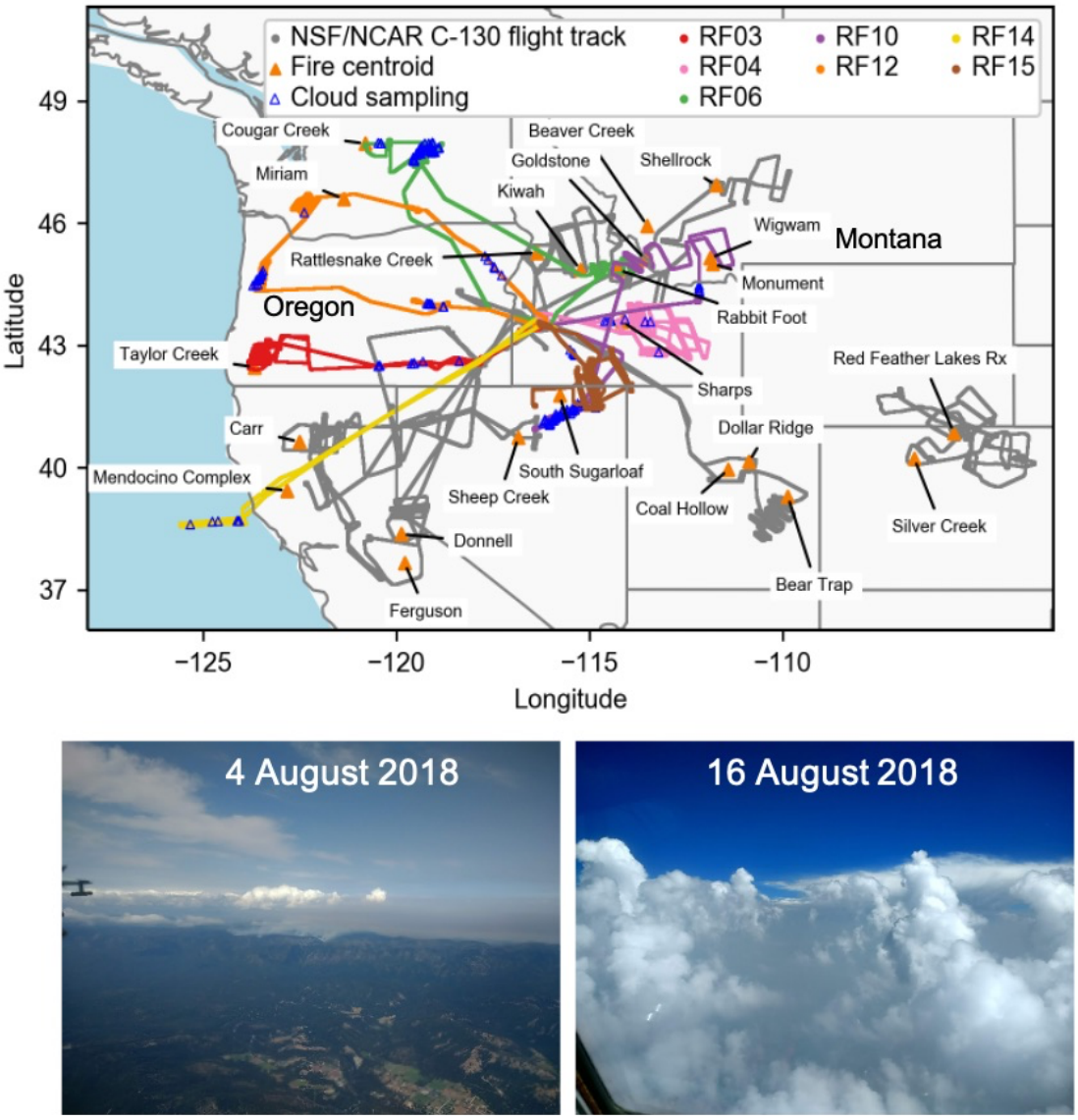

Figure 1. Top: Location of the WE-CAN sampling area over the Western U.S., with colored lines showing flights during which clouds were sampled (grey lines are other flights). Locations of clouds sampled are shown with blue triangles, while wildfires marked as orange triangles. Bottom: In-flight photos of the type of small altocumulus clouds sampled on 4 August 2018 (Flight 6, left) and 16 August 2018 (Flight 12, right). Photo credit Emily Fischer.

A broad complement of aerosol and gas-phase chemistry measurements focused on the composition and evolution of the smoke aerosol. Measurements used here include aerosol size distributions from a nano-Scanning Mobility Particle Sizer (nSMPS) [*Ortega et al.*, 2019] and Ultra High Sensitivity Aerosol Spectrometers (UHSAS) [*Kupc et al.*, 2018], as well as cloud condensation nuclei (CCN) spectra [*Roberts and Nenes*, 2005]. Refractory black carbon (rBC) content of the aerosol was obtained with a Single Particle Soot Photometer (SP2) [*Schwarz et al.*, 2006], while single scattering albedo (SSA) was derived from a photoacoustic absorption spectrometer (PAS) [*Foster et al.*, 2019] and Cavity Attenuated Phase Shift Spectroscopy (CAPS PM_{SSA}) [*Onasch et al.*, 2015]. Single particle chemical composition for selected particles was obtained via analytical Scanning Transmission Electron Microscopy (STEM) and X-ray spectroscopy, and bulk submicron aerosol composition was measured with a High-Resolution time-of-flight Aerosol Mass Spectrometer (HR-AMS) [*Garofalo et al.*, 2019]. Cloud droplet size distributions were determined with a cloud droplet probe (CDP), while larger hydrometeors were measured with a 2D-C optical array probe. Bulk cloud liquid water content was measured with a CSIRO/King hot-wire probe [*King et al.*, 1978]. More details of these instruments and their WE-CAN configuration are given in the Supporting Information.

3 Results

3.1 Cloud microphysics

Fig. 2a shows 1 Hz droplet number concentrations in smoke-impacted small cumulus clouds during the 4 flights with the most cloud penetrations. Peak concentrations were usually over 1000 cm^{-3}, and were over 3,000 cm^{-3} on Flights 6 and 10. Peak updraft velocities ranged from <1 m s^{-1} to about 7 m s^{-1}. Statistics of cloud droplet concentrations for all 7 cloud flights are shown in Fig. 2b. The following inclusion criteria was used for eligible cloud segments, where each segment was approximately 1 km long (7 sec averages): cloud liquid water content (LWC) was continually >0.01 g m^{-3} and cloud droplet number concentration was continually >10 cm^{-3} for all 7 sec. Even with these requirements, some clouds were tenuous with very low mean LWCs, so Fig. 2c shows a similar plot including just the cloud segments with mean LWCs > 0.1 g m^{-3}. Median LWC was 0.11 g m^{-3} for all cloud segments and 0.18 g m^{-3} for clouds with mean LWCs >0.1 g m^{-3}. Higher LWC clouds have stronger dynamic forcing and so more and smaller CCN are activated, leading to 40-60% higher median droplet concentrations when the higher LWC screening was used (Fig. 2b vs. Fig. 2c).

Median cross-cloud droplet concentrations were ~780 cm^{-3} for all segments (Fig. 2b, green), and 1100 cm^{-3} for segments with LWCs >0.1 g m^{-3} (Fig. 2c, green). Droplet concentrations for WE-CAN smoke-impacted clouds are thus about 5x higher than median remote continental cumulus droplet concentrations of 240 cm^{-3} measured by *Leaitch et al.* [1992] over NE North America (their median LWC was 0.24 g m^{-3} and thus more comparable to our higher LWC statistics; Fig. 2c). Peak number concentrations (median values 1250 cm^{-3} and 1960 cm^{-3}; Fig. 2b and 2c, purple) for our data set are also much higher than peak number concentrations of ~140-320 cm^{-3} reported for Washington cumulus clouds under a westerly flow regime [*Radke and Hobbs*, 1991]. While LWC was not reported for the 1991 study, WE-CAN clouds had similar temperatures and depths (most ≤ 1 km deep) as clouds in that study.

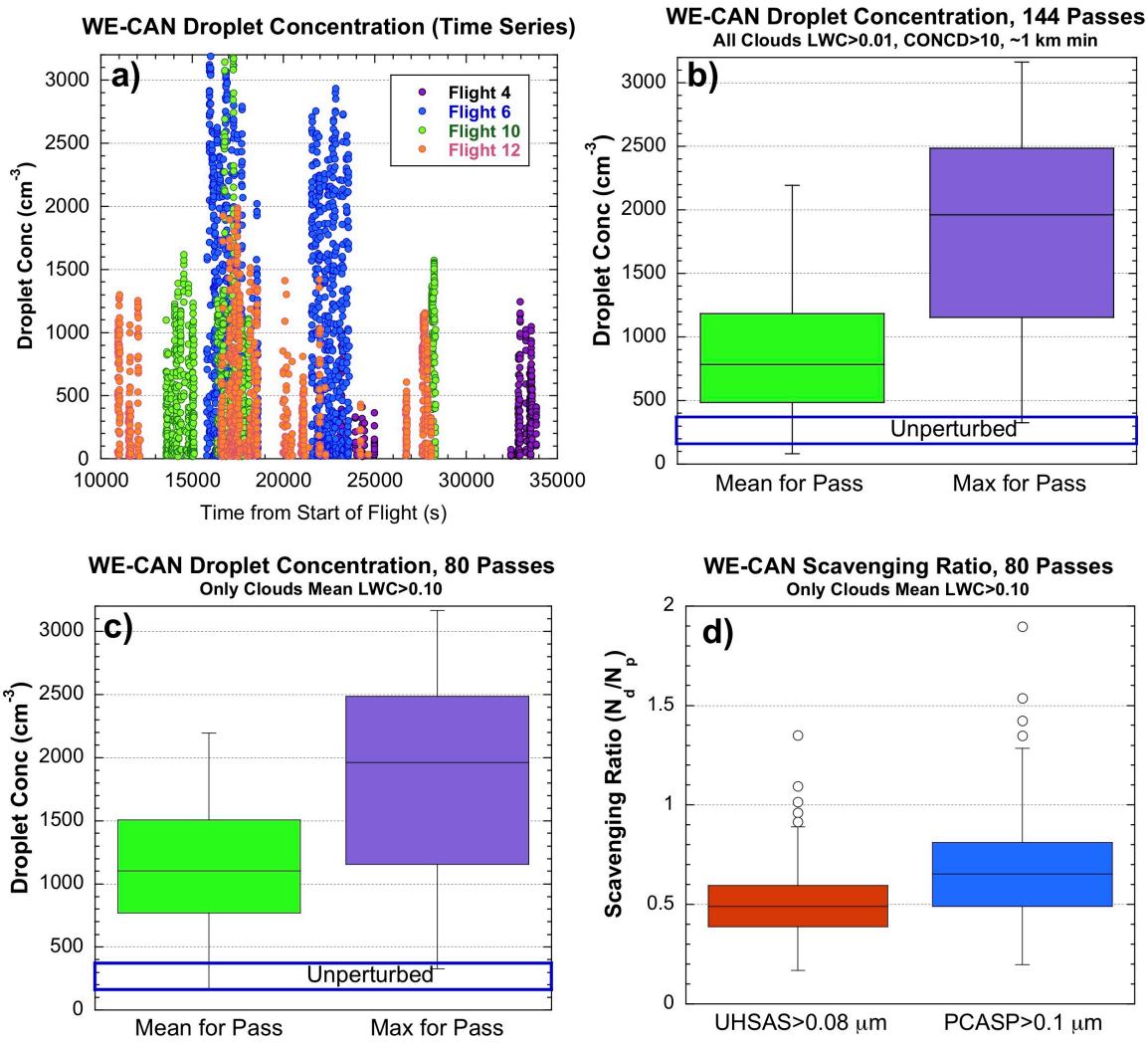

Figure 2. a) Droplet concentrations (at 1 Hz) vs time for cloud penetrations on four WE-CAN smoke-influenced flights (4, 6, 10 and 12). b) Statistical box and whisker plots of droplet concentrations on flights 3, 4, 6, 10, 12, 14, and 15 for cloud segments with droplet concentration >10 cm^{-3} and LWC > 0.01 g m^{-3} for at least 7 continuous sec. Cloud segment means are on the left in green, while maximum values at 1 Hz are on the right in purple. Colored boxes include data between lower and upper quartiles and the horizontal line is the median for all values. Outlier values (circles) extend beyond 1.5x the interquartile distance from the box; vertical lines show the full range of non-outlying values. Droplet concentrations expected in small cumulus not impacted by smoke from other studies [*Radke and Hobbs*, 1991; *Leaitch et al.*, 1992] are shown in blue boxes marked "Unperturbed". c) As in b), but restricted to cloud segments with mean LWC>0.10 g m^{-3}. d) Box plots of scavenging ratios, or number of droplets N_d divided by number of particles N_p below cloud. Ratios for particles in the wing-mounted UHSAS size range (0.08-1.0 μm diameter) are in red on left and for PCASP size range (0.10-1.0 μm diameter) are in blue on right.

For WE-CAN cumulus clouds with LWC>0.1 g m^{-3}, droplet concentrations for all cloud segments were >500 cm^{-3}, always greater than expected for unperturbed clouds. Only the off-shore stratocumulus clouds sometimes had droplet concentrations <500 cm^{-3}. This demonstrates that cumulus clouds were impacted across the sampled northwestern U. S. region (Fig. 1). Given the widespread influence of smoke during the summer season and the ability of WE-CAN smoke to act as CCN as discussed below, enhanced smoke CCN are the most likely cause of the observed high droplet concentrations.

Because of the high droplet concentrations and relatively low LWCs, cloud droplet sizes were quite small. For the 6 flights measuring small cumulus clouds, 76% of the cross-cloud mean droplet diameters were between 5-7 μm. With such small droplet sizes, coalescence and liquid-phase precipitation is expected to be minimal (see Section 4). In fact, number concentrations of particles larger than 75 μm measured by the 2D-C probe were <1 L^{-1} for 92% of the cumulus cloud segments. Flights 3, 12 and 15 (with slightly supercooled temperatures 263K-269K) had some segments with >75 μm number concentrations between 3 and 12 L^{-1}. These particles were confirmed from images to be ice. *Barry et al.* [2021] showed that smoke plumes measured during this project were associated with elevated ice nucleating particle concentrations. However, the limited sampling in clouds containing ice at a range of temperatures precludes robust conclusions on smoke impacts on ice formation during WE-CAN.

3.2 Smoke Size, Composition and Scavenging Ratios

Cloud droplet number concentrations for cloud segments as described above were compared to nearby aerosol number concentrations within the smoke layer for the wing-mounted UHSAS (0.08-1.0 μm diameter) and PCASP (0.10-1.0 μm diameter) size ranges to estimate the scavenging ratio, or fraction of smoke particles that activate into cloud droplets (Fig. 2d). Because clouds were fragmented and often obscured in the smoke, it was difficult to target a consistent distance below cloud base for aerosol sampling. Actual below-cloud flight legs ranged between 250m and 950m below the in-cloud flight legs. If flight tracks did not include legs below the clouds, aerosol concentration data were taken in the smoke layer outside of clouds, but as close as possible to the cloud legs. The scavenging ratio analysis is also restricted to data in more dilute smoke regions with UHSAS count rates below 3000 s^{-1}, where the concentration error due to coincidence is small (<5% according to the manufacturer). Also, only cloud segments with mean LWCs >0.10 μm were used, in order to minimize the potential effects of clouds that might be evaporating. As discussed above, most droplets were too small to initiate coalescence, so the assumption of a one-to-one correspondence between CCN and droplet should be acceptable.

Fig. 2d shows that in the median for all segments, about 50% of particles >0.08 μm activated and about 65% of particles >0.10 μm activated. This suggests that most smoke particles in the accumulation mode were acting as CCN, even at the relatively modest supersaturations expected in these small cumulus clouds. Note that the calculated scavenging ratios were occasionally above 1.0. This could occur if the optical probes undercounted particles near or below the lower size limit that actually formed cloud droplets, or if the altitude of the leg chosen for below cloud measurement didn't accurately represent the altitude of particles entering cloud base for that case.

In order to further understand the activation of smoke particles into droplets, an example of the below-cloud aerosol size distribution, submicron aerosol composition, and calculated aerosol hygroscopicities for aged smoke sampled on Flight 6 are shown in Fig. 3. Hygroscopicity is parameterized by the kappa value [*Petters and Kreidenweis*, 2007], which is calculated from the aerosol size distribution and CCN spectrum. This was the flight with consistently highest cloud droplet concentrations, although size distributions and hygroscopicities of smoke on other flights were similar.

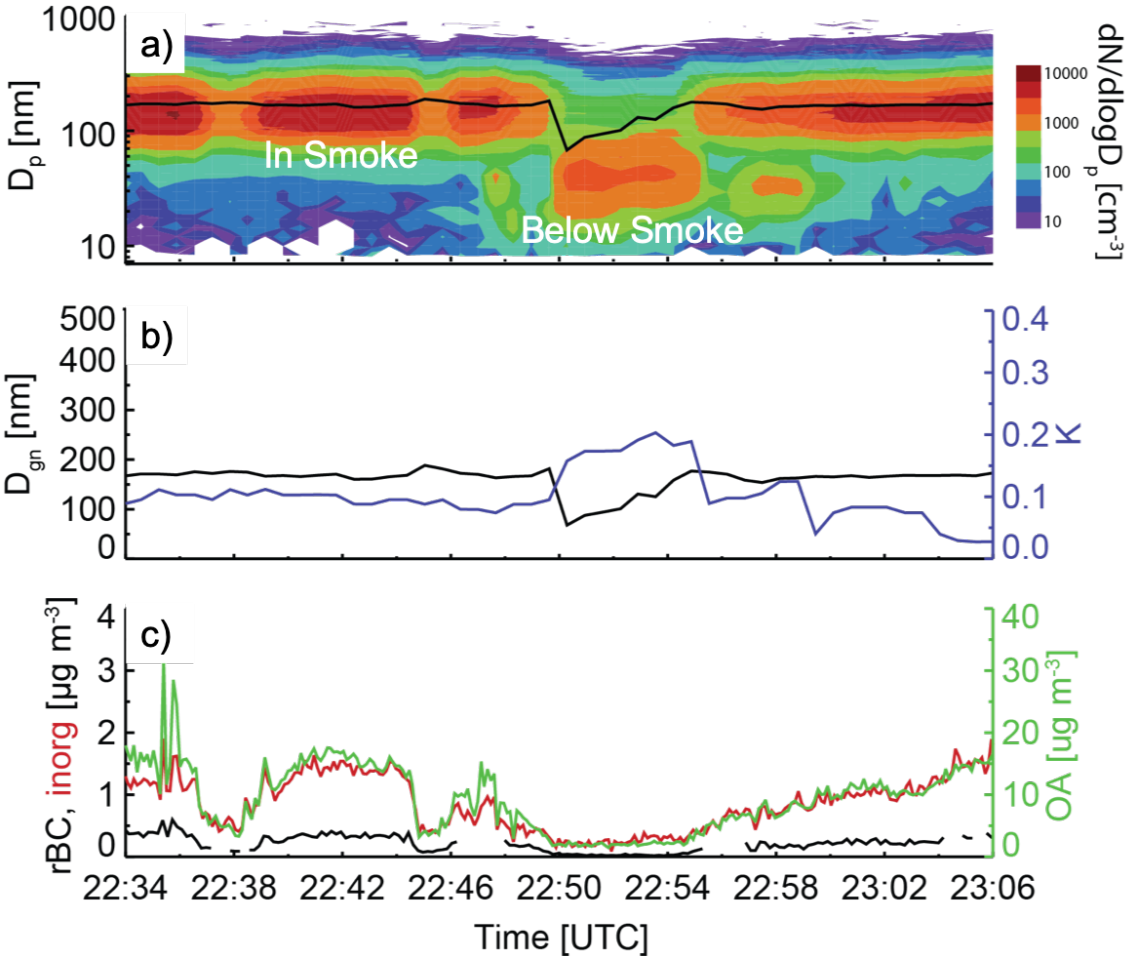

Figure 3. a) Smoke particle size distribution (nSMPS and UHSAS combined) from below-cloud leg on Flight 6 (3 August 2018) as a function of time. Vertical axis is particle diameter and colors represent particle number concentration; black line is mean aerosol diameter. The aircraft is mostly within the smoke at 2.7-2.8 km altitude, with a dip at 22:50-22:55 UTC into cleaner air at 2.1 km. b) Geometric mean number diameter (D_{gn}) and hygroscopicity parameter kappa (κ), calculated from CCN spectrum and size distribution. c) Submicron mass concentration of non-refractory organics and inorganics from the HR-AMS and refractory black carbon from the SP2.

Most smoke particles were large, predominately in the accumulation mode with a geometric mean diameter (D_{gn}) of about 170 nm for this case. The dominance of the accumulation mode was observed for fresher WE-CAN smoke plumes as well, with D_{gn} between 160-230 nm for six fire cases with smoke plume ages between 40 min and 200 min (Fig. S1). On Flight 6, when the aircraft dipped below the main smoke layer briefly at 22:50 UTC, the size distribution instead was dominated by a 20-70 nm Aitken mode. HR-AMS composition data (Fig. 3c) revealed that the non-refractory smoke aerosol was mostly organic carbon, with non-refractory inorganic aerosol comprising about 8% of the submicron mass. Refractory black carbon mass from the SP2 was about 2% of the non-refractory submicron aerosol mass, which was typical for WE-CAN flights in smoke throughout the western U.S. as reported in *Garofalo et al.* [2019].

The relatively low black carbon mass percentage is consistent with the SSA of about 0.96 (at 450 nm) and 0.97 (at 660 nm) determined from the PAS and CAPS PM_{SSA} monitor for this period. These SSA values typical of aged smoke outside of active plumes were higher than values measured in thick plumes close to fires, which were typically about 0.92-0.93. Calculated kappa values of ~0.05 to 0.15 (Fig. 3b) are consistent with an aerosol dominated by organic material and are within the range determined in prior studies of biomass burning aerosol [*Carrico et al.*, 2008; *Petters et al.*, 2009]. Despite the relatively low mean hygroscopicity, most particles are internally mixed with some hygroscopic components, as shown below. Since activation into cloud droplets to a first order is dependent on the number of solute molecules present, the relatively large mean diameter (~180 nm) of the smoke accumulation mode makes them able to act as CCN at modest supersaturations and thus impact the properties of the sampled cloud types.

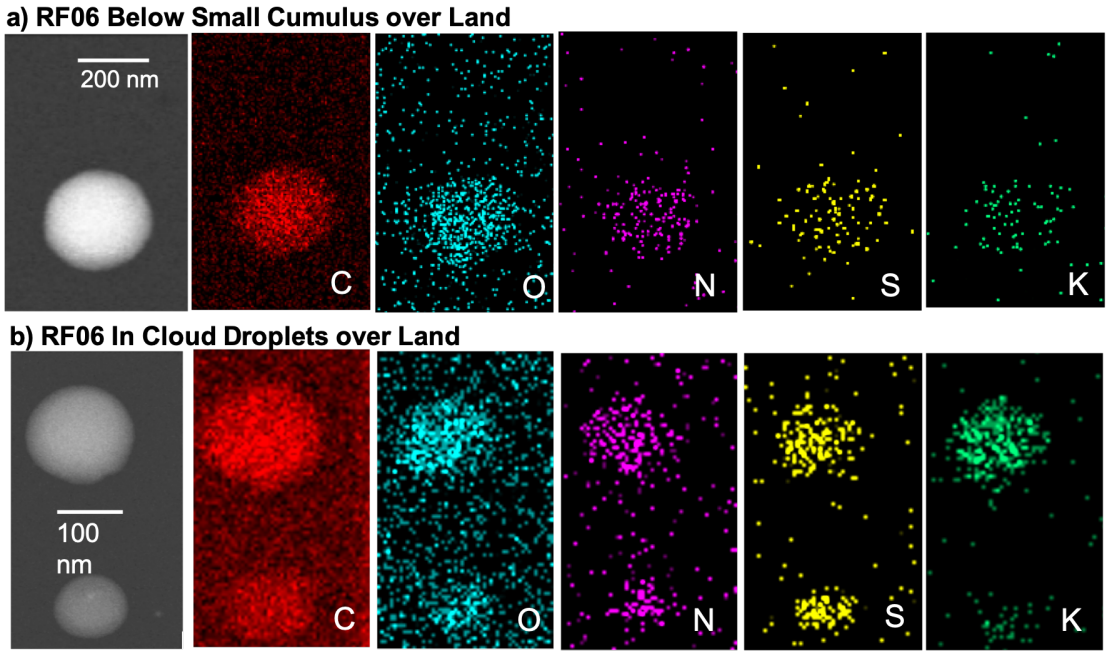

Figure 4. a) Particle bright-field image and X-ray emission mapping of Flight 6 below-cloud particle, with elements carbon, oxygen, nitrogen, sulfur, and potassium. b) As in a), but for cloud droplet residual particles sampled from small cumulus cloud droplets on the same flight.

The ability of WE-CAN biomass burning particles to act as CCN is borne out by the electron microscopy analysis of single particles from evaporated cloud droplets. Fig. 4 shows examples of aged biomass burning particles from Flight 6, with a bright-field image of particles sampled on the left and the relative intensity of X-ray emission from various elements in each row. The first row (Fig. 4a) is a typical example of aged biomass burning particles collected below clouds, where most particles contained carbon and oxygen, often internally mixed with nitrogen, sulfur and potassium, distributed throughout the particle. This morphology and composition was similar to that observed in sampling of plumes near active fires on other flights during the project, and these particles were characterized as organic biomass burning particles (see Supporting Information). Cloud residuals collected from Flight 6 (Fig. 4b) had a very similar morphology and composition. In fact, 92% of residual particles in the 0.1-0.5 μm physical diameter range analyzed from this cloud sample were this organic particle type (total n=26).

Individual particles were analyzed for four flights sampling in fire smoke plumes, aged smoke and altocumulus (n=280). Organic biomass burning particles were on average 74% by number in the 0.1-0.5 μm diameter range, followed by 13% mineral dust and metals, 8% mixtures of organics and dust, with the remaining 5% being sulfates. A small sampling of particles >0.5 μm over the western U.S. (total n=91) also were predominately organic biomass burning types, while mineral dust, ash and mixtures of these with biomass burning organics comprised about one quarter by number. Even stratocumulus clouds over the ocean off the California coast showed evidence of being impacted by smoke. 71% of residual droplets analyzed in the 0.1-0.5 μm diameter range (n=16) were identified as biomass burning derived, including those internally mixed with sea-salt-based sea-spray. This internal mixing likely occurs through in-cloud scavenging of large droplets formed on sea-spray with more numerous biomass burning particles. Coalescence of cloud droplets could also be a source of these mixed particle types, since unlike the altocumulus sampled over land, the coastal stratocumulus clouds had larger droplets where some collision/coalescence could occur.

4 Possible Regional Climate Implications

A number of complex and competing climatic impacts are possible [*Jacobson*, 2014] due to the widespread biomass-burning smoke present over the western U.S. and Canada during the summer season. Here we discuss potential effects on primarily liquid clouds that can be partially addressed with our in-situ measurements.

Smoke-impacted altocumulus clouds had about 5x the droplet concentrations of unperturbed clouds measured previously in the region (Fig. 2b,c). Due to the high droplet number concentrations, the cloud droplet effective radius r_{eff}, which together with liquid water path determines the albedo of water clouds, was typically about 4-5 μm. Given that r_{eff} is inversely proportional to $N_d^{1/3}$ [*Liu and Hallett*, 1997; *Reid et al.*, 1999], the expected r_{eff} for non-smoke impacted clouds would be about 8 μm. Thus the r_{eff} of smoke-impacted clouds is about half of that expected for pristine clouds in the region. This difference is similar to calculated changes in droplet size observed for cumulus clouds within the Amazon jungle impacted by biomass burning smoke [*Roberts et al.*, 2003].

The smaller r_{eff} for smoky clouds could increase the albedo of small cumulus clouds leading to a cooling effect, assuming a constant liquid water path. The assumption of a constant liquid water path may not be realistic for smoky clouds, however, since radiative perturbations by smoke itself can affect atmospheric stability, evapotranspiration and relative humidity, reducing cloud frequency for a net warming effect. This has been observed over the Indian Ocean and the Amazon [*Ackerman et al.*, 2000; *Koren et al.*, 2004; *Liu*, 2005]. Globally, biomass-burning aerosol absorption and semi-direct effects were predicted to outweigh indirect effects on climate, for a net positive radiative forcing [*Jacobson*, 2014]. *Ten Hoeve et al.* [2012] found that the relative importance of aerosol absorption effects vs. cloud indirect effects depended on smoke aerosol optical depth (AOD at 0.55 μm), with absorption (warming) effects dominating for smoke with AODs between ~0.3-0.9 over Amazonia. Satellite-derived AODs in the WE-CAN sampling regions were usually in this ~0.3-0.9 range. If smoke and cloud characteristics were similar to those in the *Ten Hoeve et al.* [2012] study, potential cooling effects due to smaller droplets would be overwhelmed by warming impacts of the smoke itself. However, the aged WE-CAN smoke was less absorbing and had a higher SSA (0.96-0.97) than smoke simulated in most modeling studies. For example, *Ackerman et al.* [2000] and *Liu* [2005] used a SSA of 0.88. The higher SSA in the western U.S. smoke region would decrease the aforementioned warming tendency of smoke particles, as well as any additional warming effects of smoke inside cloud droplets [*Twohy et al.*, 1989; *Chuang et al.*, 2002; *Jacobson*, 2014].

Microphysical effects on precipitation are also possible due to the reduced droplet sizes in smoke-influenced clouds. Precipitation is formed at warm temperatures through collision and coalescence when droplets reach a certain size. The probability of precipitation at the observed r_{eff} for WE-CAN clouds (4-5 μm) is virtually zero [*Freud and Rosenfeld*, 2012]. Lower precipitation rates also would be expected with smoke-induced decreases in cloud frequency for the reasons discussed in the prior section. Decreases in precipitation could in turn feed back on wildfire frequency [*Liu*, 2005], and could further stress water resources in western states such as California that are already prone to multi-year drought [USGCRP, 2017]. Western wildfire smoke also is transported eastward [*Brey et al.*, 2018] and may impact precipitation downstream as well. For example, a modeling study [*Liu*, 2005] showed that warming due to transported western U.S. smoke could weaken the low pressure troughs over the Midwest and substantially reduce precipitation there as well.

Our study measured relatively shallow altocumulus clouds, which are present in greater amounts in the summer months over the western U.S. than other cloud types [*Eastman et al.*, 2014]. In deeper clouds with higher liquid water contents that extend up to colder temperatures, effects would likely be different. For example, smoke CCN could reduce droplet size and decrease precipitation efficiency at low levels [*Freud and Rosenfeld*, 2012], while precipitation enhancement at higher altitudes can occur via mechanisms still under debate [*Cotton and Walko*, 2021]. In addition, since wildfire smoke particles serve as ice nucleating particles (INPs) under some conditions [*Levin et al.*, 2005; *McCluskey et al.*, 2014; *Sokolik et al.*, 2019; *Barry et al.*, 2021], precipitation increases are possible through this route in deeper clouds as well. In fact, *Barry et al.* [2021] found that INPs were enhanced in WE-CAN smoke plumes relative to background air outside plumes, and that organic INP dominated over biological and mineral dust under most conditions.

5 Summary and Conclusions

Smoke particles from wildfires over the western United States are composed of primarily organic and some inorganic compounds, and they frequently form droplets in small cumulus clouds due to their large size and moderately hygroscopic nature. Droplets in smoke-influenced altocumulus clouds, on average, were about 5x more numerous and about 1/2 the size of those expected for non-perturbed clouds in the same region. The more numerous and smaller droplets would increase cloud albedo and decrease the likelihood of precipitation in these shallow cumulus clouds. Radiative impacts of the smoke aerosol itself can be large and may counter these indirect aerosol effects; however this is less likely in this region given the relatively high SSA of the smoke aerosol. Effects on deep convective clouds are expected to be different as well. Together these effects likely exert a complex radiative forcing in the region that would require a detailed regional model with aerosol and cloud microphysics and radiation to assess the net effect. Statistical studies of smoke loadings versus cloud and precipitation frequency for years of record would also be valuable.

Acknowledgements

This work was supported by NSF AGS1650288 (for CHT, DWT, BW), NSF AGS1650786 (for EJL, PJD, EVF, KAM), NSF AGS1650493 (for RP, SMM) and NOAA Climate Program Office grant NA17OAR4310010 (for DKF, LAG, MAP, and SMK). KAM was supported by an NSF Graduate Research Fellowship (Grant No. 006784). Any opinions, findings, and conclusions or recommendations expressed in this material are those of the authors and do not necessarily reflect the views of the National Science Foundation. Roy Geiss at Colorado State University performed the STEM analysis. We thank the crew of the NSF C-130 aircraft, Drs. Darrel Baumgardner and Jorgen Jensen for helpful discussions, Adriana Bailey and Stephanie Redfern who assisted with particle sampling and Julieta Juncosa Calahorrano for the creation of Fig. 1. Aircraft data are available at https://data.eol.ucar.edu/project/WE-CAN. One-day MODIS AODs (Section 4) were taken from the NASA Earth Observations site at https://neo.sci.gsfc.nasa.gov/view.php?datasetId=MYDAL2_D_AER_OD.

References

Abatzoglou, J. T., and A. P. Williams (2016), Impact of anthropogenic climate change on wildfire across western US forests, *Proceedings of the National Academy of Sciences*, *113*(42), 11770.

Ackerman, A. S., O. B. Toon, D. E. Stevens, A. J. Heymsfield, V. Ramanathan, and E. J. Welton (2000), Reduction of tropical cloudiness by soot, *Science*, *288*(5468), 1042-1047.

Andreae, M. O., D. Rosenfeld, P. Artaxo, A. A. Costa, G. P. Frank, K. N. Longo, and M. A. F. Silva-Dias (2004), Smoking rain clouds over the Amazon, *Science*, *303*, 1337-1342.

Barry, K. R., et al. (2021), Observations of Ice Nucleating Particles in the Free Troposphere From Western US Wildfires, *J. Geophys. Res. Atmos.*, *126*(3), e2020JD033752.

Brey, S. J., M. Ruminski, S. A. Atwood, and E. V. Fischer (2018), Connecting smoke plumes to sources using Hazard Mapping System (HMS) smoke and fire location data over North America, *Atmos. Chem. Phys.*, *18*(3), 1745-1761.

Brey, S. J., E. A. Barnes, J. R. Pierce, A. L. S. Swann, and E. V. Fischer (2020), Past variance and future projections of the environmental conditions driving western U.S. summertime wildfire burn area, *Earth's Future*, *n/a*(n/a), e2020EF001645.

Carrico, C. M., M. D. Petters, S. M. Kreidenweis, J. L. Collett Jr, G. Engling, and W. C. Malm (2008), Aerosol hygroscopicity and cloud droplet activation of extracts of filters from biomass burning experiments, *J. Geophys. Res. Atmos.*, *113*(D8).

Chuang, C. C., J. E. Penner, J. M. Prospero, K. E. Grant, G. H. Rau, and K. Kawamoto (2002), Cloud susceptibility and the first aerosol indirect forcing: Sensitivity to black carbon and aerosol concentrations, *J. Geophys. Res. Atmos.*, *107*(D21), AAC 10-11-AAC 10-23.

Cotton, W. R., and R. Walko (2021), Examination of Aerosol-Induced Convective Invigoration Using Idealized Simulations, *J. Atmos. Sci.*, *78*(1), 287-298.

Dennison, P. E., S. C. Brewer, J. D. Arnold, and M. A. Moritz (2014), Large wildfire trends in the western United States, 1984–2011, *Geophys. Res. Lett.*, *41*(8), 2928-2933.

Eagan, R. C., P. V. Hobbs, and L. F. Radke (1974), Measurements of Cloud Condensation Nuclei and Cloud Droplet Size Distributions in the Vicinity of Forest Fires, *J. Appl. Meteorol.*, *13*(5), 553-557.

Eastman, R., S. G. Warren, and C. J. q. Hahn (2014), Climatic Atlas of Clouds Over Land and Ocean, edited, https://atmos.uw.edu/CloudMap/.

Foster, K., R. Pokhrel, M. Burkhart, and S. Murphy (2019), A novel approach to calibrating a photoacoustic absorption spectrometer using polydisperse absorbing aerosol, *Atmos. Meas. Tech.*, *12*(6), 3351-3363.

Freud, E., and D. Rosenfeld (2012), Linear relation between convective cloud drop number concentration and depth for rain initiation, *J. Geophys. Res.*, *117*, D02207.

Gao, S., D. A. Hegg, P. V. Hobbs, T. W. Kirchstetter, B. I. Magi, and M. Sadilek (2003), Water-soluble organic components in aerosols associated with savanna fires in southern Africa: Identification, evolution, and distribution, *J. Geophys. Res. Atmos.*, *108*(D13).

Garofalo, L. A., M. A. Pothier, E. J. T. Levin, T. Campos, S. M. Kreidenweis, and D. K. Farmer (2019), Emission and Evolution of Submicron Organic Aerosol in Smoke from Wildfires in the Western United States, *ACS Earth and Space Chemistry*, *3*(7), 1237-1247.

Gomez, S. L., et al. (2018), Southwestern U.S. Biomass Burning Smoke Hygroscopicity: The Role of Plant Phenology, Chemical Composition, and Combustion Properties, *J. Geophys. Res. Atmos.*, *123*(10), 5416-5432.

Jacobson, M. Z. (2014), Effects of biomass burning on climate, accounting for heat and moisture fluxes, black and brown carbon, and cloud absorption effects, *J. Geophys. Res. Atmos.*, *119*(14), 8980-9002.

King, W. D., D. A. Parkin, and R. J. Handsworth (1978), A Hot-Wire Liquid Water Device Having Fully Calculable Response Characteristics, *J. Appl. Meteorol.*, *17*(12), 1809-1813.

Koren, I., Y. J. Kaufman, L. A. Remer, and J. V. Martins (2004), Measurement of the Effect of Amazon Smoke on Inhibition of Cloud Formation, *Science*, *303*(5662), 1342.

Künzli, N., et al. (2006), Health effects of the 2003 Southern California wildfires on children, *Am J Respir Crit Care Med*, *174*(11), 1221-1228.

Kupc, A., C. Williamson, N. L. Wagner, M. Richardson, and C. A. Brock (2018), Modification, calibration, and performance of the Ultra-High Sensitivity Aerosol Spectrometer for particle size distribution and volatility measurements during the Atmospheric Tomography Mission (ATom) airborne campaign, *Atmos. Meas. Tech.*, *11*(1), 369-383.

Lance, S., C. A. Brock, D. Rogers, and J. A. Gordon (2010), Water droplet calibration of the Cloud Droplet Probe (CDP) and in-flight performance in liquid, ice and mixed-phase clouds during ARCPAC, *Atmospheric Measurement Techniques*, *3*(6), 1683-1706.

Leaitch, W. R., G. A. Isaac, J. W. Strapp, C. M. Banic, and H. A. Wiebe (1992), The relationship between cloud droplet number concentrations and anthropogenic pollution: Observations and climatic implications, *J. Geophys. Res. Atmos.*, *97*(D2), 2463-2474.

Levin, Z., A. Teller, E. Ganor, and Y. Y (2005), On the interactions of mineral dust, sea-salt particles, and clouds: A measurement and modeling study from the Mediterranean Israeli Dust Experiment campaign, *J. Geophys. Res.*, *110*(D20).

Li, J., M. Pósfai, P. V. Hobbs, and P. R. Buseck (2003), Individual aerosol particles from biomass burning in southern Africa: 2, Compositions and aging of inorganic particles, *J. Geophys. Res. Atmos.*, *108*(D13).

Liu, Y. (2005), Atmospheric response and feedback to radiative forcing from biomass burning in tropical South America, *Agricultural and Forest Meteorology*, *133*(1), 40-53.

Liu, Y., and J. Hallett (1997), The '1/3' power law between effective radius and liquid-water content, *Q J Roy Meteor Soc*, *123*(542), 1789-1795.

McCluskey, C. S., P. J. DeMott, A. J. Prenni, E. J. T. Levin, G. R. McMeeking, A. P. Sullivan, T. C. J. Hill, S. Nakao, C. M. Carrico, and S. M. Kreidenweis (2014), Characteristics of atmospheric ice nucleating particles associated with biomass burning in the US: Prescribed burns and wildfires, *J. Geophys. Res. Atmos.*, *119*(17), 10458-10470.

McFarquhar, G. M., et al. (2017), Processing of Ice Cloud In Situ Data Collected by Bulk Water, Scattering, and Imaging Probes: Fundamentals, Uncertainties, and Efforts toward Consistency, *Meteorological Monographs*, *58*, 11.11-11.33.

McNaughton, C. S., et al. (2007), Results from the DC-8 Inlet Characterization Experiment (DICE): airborne versus surface sampling of mineral dust and sea salt aerosols, *Aerosol Sci Tech*, *41*(2), 136-159.

Noone, K. J., J. A. Ogren, J. Heintzenberg, R. J. Charlson, and D. S. Covert (1988), Design and calibration of a Counterflow Virtual Impactor for sampling of atmospheric fog and cloud droplets, *Aerosol Sci. Technol.*, *8*(3), 235-244.

Onasch, T. B., P. Massoli, P. L. Kebabian, F. B. Hills, F. W. Bacon, and A. Freedman (2015), Single Scattering Albedo Monitor for Airborne Particulates, *Aerosol Sci Tech*, *49*(4), 267-279.

Ortega, J., J. R. Snider, J. N. Smith, and J. M. Reeves (2019), Comparison of aerosol measurement systems during the 2016 airborne ARISTO campaign, *Aerosol Sci Tech*, *53*(8), 871-885.

Petters, M. D., and S. M. Kreidenweis (2007), A single parameter representation of hygroscopic growth and cloud condensation nucleus activity, *Atmos. Chem. Phys.*, *7*(8), 1961-1971.

Petters, M. D., C. M. Carrico, S. M. Kreidenweis, A. J. Prenni, P. J. DeMott, J. L. Collett Jr, and H. Moosmüller (2009), Cloud condensation nucleation activity of biomass burning aerosol, *J. Geophys. Res. Atmos.*, *114*(D22).

Radke, L. F., and P. V. Hobbs (1991), Humidity and particle fields around some small cumulus clouds, *J. Atmos. Sci.*, *48*(9), 1190-1193.

Reid, J. S., P. V. Hobbs, A. L. Rangno, and D. A. Hegg (1999), Relationships between cloud droplet effective radius, liquid water content, and droplet concentration for warm clouds in Brazil embedded in biomass smoke, *J. Geophys. Res. Atmos.*, *104*(D6), 6145-6153.

Reid, J. S., R. Koppmann, T. F. Eck, and D. P. Eleuterio (2005), A review of biomass burning emissions part II: intensive physical properties of biomass burning particles, *Atmos. Chem. Phys.*, *5*(3), 799-825.

Roberts, G. C., and A. Nenes (2005), A Continuous-Flow Streamwise Thermal-Gradient CCN Chamber for Atmospheric Measurements, *Aerosol Sci Tech*, *39*(3), 206-221.

Roberts, G. C., A. Nenes, J. H. Seinfeld, and M. O. Andreae (2003), Impact of biomass burning on cloud properties in the Amazon Basin, *J. Geophys. Res. Atmos.*, *108*(D2).

Ross, K. E., S. J. Piketh, R. T. Bruintjes, R. P. Burger, R. J. Swap, and H. J. Annegarn (2003), Spatial and seasonal variations in CCN distribution and the aerosol-CCN relationship over southern Africa, *J. Geophys. Res. Atmos.*, *108*(D13).

Ruellan, S., H. Cachier, A. Gaudichet, P. Masclet, and J.-P. Lacaux (1999), Airborne aerosols over central Africa during the Experiment for Regional Sources and Sinks of Oxidants (EXPRESSO), *J. Geophys. Res. Atmos.*, *104*(D23), 30673-30690.

Schwarz, J. P., et al. (2006), Single-particle measurements of midlatitude black carbon and light-scattering aerosols from the boundary layer to the lower stratosphere, *J. Geophys. Res. Atmos.*, *111*(D16).

Sokolik, I. N., A. J. Soja, P. J. DeMott, and D. Winker (2019), Progress and Challenges in Quantifying Wildfire Smoke Emissions, Their Properties, Transport, and Atmospheric Impacts, *J. Geophys. Res. Atmos.*, *124*(23), 13005-13025.

Ten Hoeve, J. E., M. Z. Jacobson, and L. A. Remer (2012), Comparing results from a physical model with satellite and in situ observations to determine whether biomass burning aerosols over the Amazon brighten or burn off clouds, *J. Geophys. Res. Atmos.*, *117*(D8).

Twohy, C. H., J. W. Strapp, and M. Wendisch (2003), Performance of a counterflow virtual impactor in the NASA Icing Research Tunnel, *J. Atmos. Ocean. Tech.*, *20*(6), 781-790.

Twohy, C. H., A. D. Clarke, S. G. Warren, L. F. Radke, and R. J. Charlson (1989), Light-Absorbing Material Extracted from Cloud Droplets and Its Effect on Cloud Albedo, *J Geophys Res-Atmos*, *94*(D6), 8623-8631.

Warner, J., and S. Twomey (1967), The Production of Cloud Nuclei by Cane Fires and the Effect on Cloud Droplet Concentration, *J. Atmos. Sci.*, *24*(6), 704-706.

Westerling, A. L. (2016), Increasing western US forest wildfire activity: sensitivity to changes in the timing of spring, *Philosophical Transactions of the Royal Society B: Biological Sciences*, *371*(1696), 20150178.

Westerling, A. L., H. G. Hidalgo, D. R. Cayan, and T. W. Swetnam (2006), Warming and Earlier Spring Increase Western U.S. Forest Wildfire Activity, *Science*, *313*(5789), 940.